

Microstructure characterization and thermal stability of the ball milled iron powders

Sonia Azzaza · Safia Alleg · Joan-Josep Suñol

Received: 7 May 2014 / Accepted: 2 November 2014 / Published online: 30 November 2014
© Akadémiai Kiadó, Budapest, Hungary 2014

Abstract X-ray diffraction and thermal measurements were used to investigate the microstructural, structural, and thermal properties of nanocrystalline Fe prepared by ball milling process. The crystallite size refinement down to the nanometer scale is accompanied by the increase of the internal level strains and the dislocations density. The lattice distortion is evidenced by the increase of both the lattice parameter and the static Debye–Waller parameter. The grain boundary enthalpy decreases above 12 h of milling. The nanostructured paramagnetic bcc α -Fe domain is extended by about 75 K at the expense of both the magnetic bcc α -Fe and nonmagnetic fcc γ -Fe domains as compared to coarse-grained pure α -Fe.

Keywords Nanomaterials · Iron powders · Microstructure · X-ray diffraction · Thermal analysis

Introduction

Nanostructured materials (NSM) are characterized by a particular nanometer-scale microstructure and an important

grain boundaries (GBs) surface area. Because of the large number of crystalline interfaces, it was suggested that an important fraction of the materials has disordered microstructure with no short-range order, which is comparable with a gas-phase structure [1]. Therefore, NSM exhibit excellent physical, magnetic, mechanical, and chemical properties that are different from those of coarse-grained crystalline or amorphous alloys [2].

Ball milling (BM) has been applied in synthesizing nanocrystalline (NC) metals, solid solutions, alloys, and intermetallics [2–4]. During the milling process, materials are subjected to high-energy impacts through ball-to-ball and/or ball-to-vial wall collisions of the grinding media. The obtained nanostructured powders consist of particles composed of nanometer size grains linked to each other through GBs. The structure of GBs, which has been controversially debated, can be viewed as heterogeneous and partially disordered systems with a significant fraction of defects.

Among the many metallic systems processed by ball milling, Fe is of particular interest. Iron is paramagnetic above T_c (1,043 K) and still bcc. In the nanostructured pure iron, a different magnetic response is observed compared to that of bulk iron, especially at low temperatures. The observed magnetic anomalies have been interpreted in terms of spin-glass-like behavior [5]. A reduction of saturated magnetic moment of nanostructured Fe is observed. These changes have been explained on the basis of the reduced size of the nanograins and the high amount of atoms at the interfaces [6]. The early studies of nanocrystalline Fe by X-ray diffraction (XRD) suggested a wide, disordered GB component without noticeable atomic short-range order [1]. These findings were supported by results from EXAFS spectroscopy evidencing a large reduction in nearest neighbor coordination number [7]. Taking into

S. Azzaza (✉)
Department of Technology, Faculty of Technology, University
20 Août 1955 of Skikda, B. P. 26, Route d'El-Hadaiek,
21000 Skikda, Algeria
e-mail: s.azzaza@gmail.com

S. Azzaza · S. Alleg
Laboratory of Magnetism and Spectroscopy of Solids,
Department of Physics, Faculty of Science, University Badji
Mokhtar of Annaba, B. P. 12, 23000 Annaba, Algeria

J.-J. Suñol
GRMT, Departamento de Física, Universitat de Girona,
Santaló s/n 17071, Girona, Spain

account all these features, a precise knowledge of the microstructure is of crucial importance for the complete understanding of the magnetic behavior.

In the present paper, the evolution of microstructural and thermal properties of ball milled pure Fe is discussed as a function of milling time.

Experimental

Elemental pure iron powder (purity, 99.9%) was milled in a planetary ball mill (Fritsch Pulverisette P7) under argon atmosphere using hardened steel containers and balls. The rotation speed was 350 rpm and the powder-to-ball mass ratio was about 2:30. Microstructural evolution during the milling process was followed by XRD using a D501 Siemens diffractometer in Bragg–Brentano ($\theta - 2\theta$) geometry by using a $\text{CuK}\alpha$ radiation of 0.154056 nm wavelength, a Ni filter, a graphite monochromator, and a proportional detector. The diffraction profiles of the unmilled and milled samples were obtained by varying 2θ from 20° to 110° with a step scan of 0.02° and a counting time of 20 s. The standard corundum Al_2O_3 was used as the standard sample to estimate the instrumental parameters like 2θ correction, peak asymmetry, and peak broadening parameters (U , V , and W). It was also assumed that Al_2O_3 standard specimen did not have any size and/or strain broadening. Structural and microstructural parameters were obtained from the Rietveld refinement of the XRD patterns by using the MAUD program which combines the Rietveld method and the Fourier analysis to describe the broadening of Bragg peaks [8, 9]. Since the nanocrystalline materials present high amount of defect density and strain anisotropy, the modified Williamson–Hall (MWH) method, which is limited to cubic crystals, is also used to estimate the density and character of dislocations during milling.

The thermal characterization was carried out by differential scanning calorimetry (DSC) in a DSC30 equipment of Mettler-Toledo and by thermogravimetry (TG) in a TGA851 Mettler-Toledo equipment. The sample mass used in thermal studies was about 100 mg. The milled Fe powders were heated under argon atmosphere to avoid oxidation at a continuous heating rate of 10 K min^{-1} .

Methods of analysis

Diffraction methods are very powerful tools for the characterization of nanocrystalline phases. Adequate phase identification using XRD relies not only on the position and the intensity of the peaks but also takes into account the width and the shape of the peaks. Those later facilitate the characterization of defects, scattering domain size distribution, and even the thermal oscillations of atoms.

In the present study, we have adopted the Rietveld's structure and microstructure refinement method [8–10] of X-ray powder diffraction step scan data to obtain the refined structural and microstructural parameters. For instrumental broadening correction, a specially processed Al_2O_3 standard was taken as the instrumental standard and the most suitable pseudo-Voigt analytical function [11] is adopted for the fitting of the experimental profiles. The variation of full width at half maximum (H) of the Al_2O_3 reflection was assumed to follow Caglioti relation [12]:

$$H^2 = U \tan^2 \theta + V \tan \theta + W. \quad (1)$$

The U , V , and W parameters of instrumental broadening, instrumental asymmetry, and Gaussianity of reflections were evaluated for the present setting of the instrument using this standard Al_2O_3 . All these instrumental parameters were incorporated in the convolution fitting process and the values were kept fixed.

After the refinement of the instrumental parameters, the positions of the peaks are corrected by successive refinements for systematic errors taking into account the zero shift error and sample displacement error. The background is refined as a four-degree polynomial followed by the refinement of the crystal structure parameters such as the lattice parameters, the atomic coordinates, and the Debye–Waller factor. When the profiles broadening are Miller indices ($h k l$) dependent, the crystallite size, d , and microstrain, $\langle \sigma^2 \rangle^{1/2}$, are evaluated from anisotropic model based on the Popa rules [13, 14]. This model is applied assuming that the crystallite and the microstrain fields have ellipsoidal shape. All the parameters are refined by an iterative least-square minimization.

The Marquardt least squares procedure was adopted for minimizing the difference between the observed and simulated powder diffraction patterns and the minimization was carried out by using the reliability index parameter; R_{wp} (weighted residual error) and R_{B} (Bragg factor) defined as

$$R_{\text{wp}} = \left[\frac{\sum_i w_i (I_0 - I_c)^2}{\sum_i w_i I_0^2} \right]^{1/2} \quad (2)$$

and

$$R_{\text{B}} = 100 \frac{\sum |I_0 - I_c|}{\sum I_0}. \quad (3)$$

The goodness of fit (GoF) is established by comparing R_{wp} with the expected error, R_{exp} :

$$R_{\text{exp}} = \left[\frac{N - P}{\sum_i w_i I_0^2} \right]^{1/2}, \quad (4)$$

where I_0 and I_c are the experimental and calculated intensities, respectively; $w_i = 1/I_0$ and N are the mass and

number of experimental observations, and P is the number of fitting parameters. This leads to the value of goodness of fit, GoF [8, 9]:

$$\text{GoF} = \frac{R_{\text{wp}}}{R_{\text{exp}}}. \tag{5}$$

Refinement continue till convergence is reached with the value of the quality factor, GoF very close to 1 (varies between 1.05 and 1.2) which confirms the goodness of fitting between I_o and I_c .

Dislocation density and character

The characterization of dislocation substructure using XRD data has received much attention. Many methods have been proposed to extract the density and character of dislocation (screw or edge) by fitting model/theoretical functions to the diffraction profiles. The dislocation densities for each sample were determined by using the Modified Williamson–Hall (MWH) method. In this method, the interpretation of the strain broadening is based on the dislocation model of the mean square strain. Here we note that from the present evaluation procedure only the overall average of dislocation densities was obtained (isotropic case). The determination of the geometrically necessary dislocations density would involve measurements of the Rocking-curves; however, this was not the goal of the present research. Hence, by using the values of the average crystallite size, $\langle d \rangle$, and average r.m.s strains, $\langle \sigma^2 \rangle^{1/2}$, that are deduced from the Rietveld refinement, the average dislocation density ρ_D values is evaluated following the same procedure as adopted in some X-ray line broadening analyses [15]:

$$\rho_D = \frac{2\sqrt{3} \langle \sigma^2 \rangle^{1/2}}{\langle d \rangle b}, \tag{6}$$

where b is the Burger’s vector which describes the magnitude and the direction of lattice distortions. The direction of b depends on the plane of dislocation which is usually on the closet-packed plane of unit cell. In the case of bcc-Fe, the closet-packed plane is (111). The magnitude of b is given by

$$b = \frac{a}{2} \sqrt{h^2 + k^2 + l^2}, \tag{7}$$

where a is the unit cell length of the crystal; h , k , and l are Miller indices.

In order to determine the character of dislocations, we have also supposed coherent domains with isotropic size. In fact, the XRD results were analyzed according to the model proposed by Ungár et al. [16] which is based on the modified Williamson–Hall plot:

$$\Delta K = \frac{0.9}{d} + \beta K \bar{C}^{1/2} + O(K^2 \bar{C}), \tag{8}$$

where $K = 2 \sin\theta/\lambda$, ΔK is the H (full width at half maximum); β the constant depending on the effective outer cut-off radius of dislocations, the Burgers vector and the density of dislocations. \bar{C} is the average contrast factor of dislocations given by

$$\bar{C} = \bar{C}_{\text{h00}}(1 - qH^2) \tag{9}$$

with

$$H^2 = \left(h^2k^2 + h^2l^2 + k^2l^2 / (h^2 + k^2 + l^2)^2 \right) \tag{10}$$

\bar{C}_{h00} values have been calculated for bcc systems as a function of elastic constant C_{11} , C_{22} and C_{44} [16]. q is related to the nature of the dislocations (screw or edge) and can be deduced directly from the line profile analysis of the diffraction pattern. Indeed inserting (9) into the quadratic form of (8) yields

$$\frac{(\Delta K)^2 - \alpha}{K^2} = \beta \bar{C}_{\text{h00}}(1 - qH^2). \tag{11}$$

From the linear regression of the left-hand side of Eq. (11) versus H^2 , the parameter q can be determined. The values used for the calculation of this parameter (q) for pure edge and pure screw dislocations are $2C_{44}/(C_{11} - C_{12}) = 2.416$ and $C_{12}/C_{44} = 1.215$. The value of \bar{C}_{200} for pure iron was calculated using the program ANIZC [17]. It has been demonstrated that the value of \bar{C}_{200} for most materials does not change significantly for different types/nature (screw or edge) of dislocations [18]. In the ‘MarqX’ [19] program, the average value of 0.3 can be used for most materials (cubic) and can be refined since small variations in the value of \bar{C}_{200} do not directly affect the refined values of q (nature of dislocations) [18, 19].

Results and discussion

Microstructure

XRD analysis can provide information on the structural and microstructural characteristics of materials since the width and the intensity of the diffraction peaks depend on lattice strain, crystallite size, and other imperfections in the powders such as stacking faults. The accuracy of the XRD measurements is crucial to the quantitative analysis for crystallite size and microstrains which are an essential requirement for quantitative studies of NC materials.

The XRD patterns of the ball-milled Fe powders showed that the diffraction peaks become substantially broadened and reduced in intensity. The $\langle 110 \rangle$ Bragg diffraction peak

Fig. 1 Evolution of the $\langle 110 \rangle$ Bragg peaks for un-milled sample and for a sample milled for 9 and 24 h versus q . $q = 2/\lambda (\sin\theta - \sin\theta_0)$ where θ is the diffraction angle and θ_0 is the exact Bragg angle

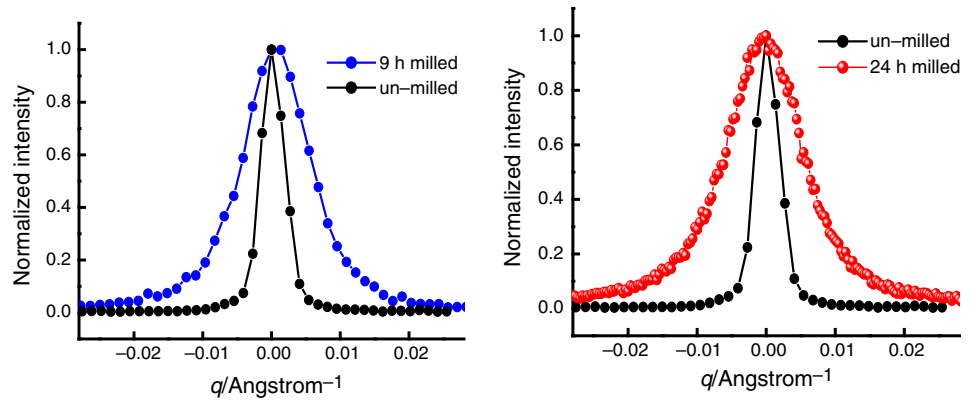


Fig. 2 Rietveld refinement of the XRD pattern of the milled Fe powders for 3, 6 and 12 h. Experimental (*dots*) and calculated (*full line*) patterns are shown. Difference is given below

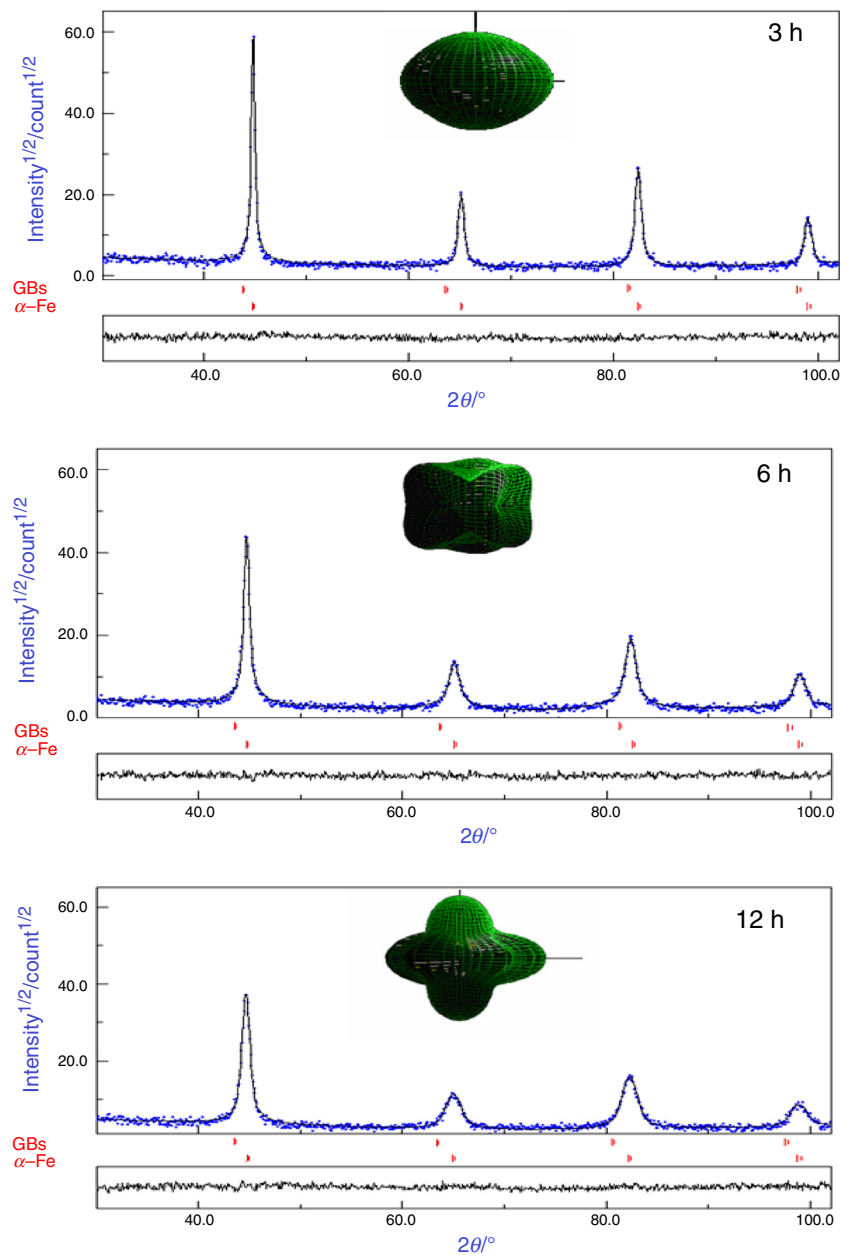


Table 1 Quality factors of fitting

Milling time/h	0	3	6	9	12	24
GoF	1.03	1.08	1.00	1.20	1.07	1.05
R _B /%	4.87	3.72	5.77	6.02	4.89	5.09
R _{wp} /%	10.12	7.13	10.18	9.46	7.44	8.14
R _{exp} /%	9.83	6.59	10.14	7.87	6.94	7.72

of un-milled and ball milled powders for 9 and 24 h is shown in Fig. 1. This broadening can be attributed to the decrease of crystallites size and the increase in the lattice distortion. Both features originate from the repeated fracturing and cold welding of particles and are explained by their large plastic deformation. Indeed, it is observed that the $\langle 200 \rangle$ peak broaden much more as compared to other peaks. This could be due to slight tetragonal distortion [20] or to the difference in the elastic modulus of the single crystal Fe in $\langle 200 \rangle$ crystallographic direction [21]. This elastic anisotropy gives rise to strain anisotropy (dislocation model of strain anisotropy) [16]. According to the anisotropic model, the best Rietveld refinement of the XRD patterns is obtained with two components: one attributed to crystalline grains and the other to the GBs (Fig. 2). This model was firstly established by Lutterotti et al. [8] to quantify the amorphous fraction in ceramic materials containing a glassy phase. It was also used by Guérault et al. to estimate the GBs concentration in NC fluoride powders [22]. Within the framework of this model, the GBs phase is considered as a NC solid where the long-range order is lost. The crystallites are hence of the same order of the cell and the r.m.s. microstrain is then neglected and set equal to zero. The quality factors of fitting, GoF, also corroborated the above findings (Table 1).

The anisotropic model suggests an anisotropic distribution of the microstructural parameters as confirmed by the non-spherical grain shape (see inset in Fig. 2). This graphical representation of the three-dimensional size distribution at different milling times may be attributed to the heterogeneous arrangement of dislocation in the powders, resulting from the cellular structure developed during plastic deformation.

The crystallite size, d , and r.m.s. (root mean square) microstrains for different $\langle hkl \rangle$ directions are presented in Table 2. d is found to be lower along the $\langle 200 \rangle$ direction. Accordingly, $\langle \sigma^2 \rangle^{1/2}$ is higher along this direction. This behavior was also observed in ball-milled Fe–30Co [23] and in pure Fe [21]. It is probably due to the elastic modulus of bcc-Fe (Table 2). It is observed that the crystallite size decreases with milling time and levels off after 12 h. The minimum average crystallite size has been attributed to a balance between the formation of dislocation structure and its recovery by thermal processes [24]. The dislocations density, ρ_D , of the Fe powders is plotted versus

Table 2 Crystallite size, $\langle d \rangle$, and r.m.s. microstrain, $\langle \sigma^2 \rangle^{1/2}$, as derived from the refinement of the XRD patterns with the anisotropic model

Milling time/h		$\langle hkl \rangle$ directions			
		$\langle 110 \rangle$	$\langle 200 \rangle$	$\langle 211 \rangle$	$\langle 310 \rangle$
0	$\langle d \rangle \pm 2/\text{nm}$	246.6	209.7	246.6	212.7
	$\langle \sigma^2 \rangle^{1/2} \pm 0.02/\%$	0.0242	0.038	0.024	0.029
3	$\langle d \rangle \pm 1/\text{nm}$	72.57	59.6	72.57	64.01
	$\langle \sigma^2 \rangle^{1/2} \pm 0.03/\%$	0.233	0.394	0.233	0.345
6	$\langle d \rangle \pm 1/\text{nm}$	39.60	21.42	39.60	28.39
	$\langle \sigma^2 \rangle^{1/2} \pm 0.02/\%$	0.412	0.517	0.412	0.491
9	$\langle d \rangle \pm 1/\text{nm}$	16.6	13.02	16.6	14.32
	$\langle \sigma^2 \rangle^{1/2} \pm 0.01/\%$	0.674	0.881	0.674	0.760
12	$\langle d \rangle \pm 2/\text{nm}$	12.37	11.15	12.37	11.92
	$\langle \sigma^2 \rangle^{1/2} \pm 0.03/\%$	0.872	1.024	0.872	0.905
24	$\langle d \rangle \pm 1/\text{nm}$	12.08	11.01	12.08	11.75
	$\langle \sigma^2 \rangle^{1/2} \pm 0.04/\%$	0.930	1.031	0.930	0.931

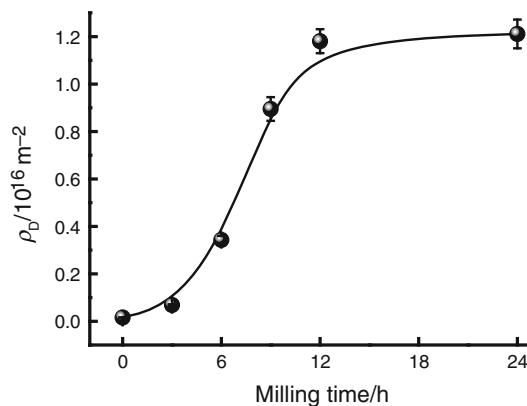


Fig. 3 Evolution of dislocations density versus milling time

milling time in Fig. 3. One observes that ρ_D increases from $0.015 \times 10^{16} \text{ m}^{-2}$ to about $1.21 \times 10^{16} \text{ m}^{-2}$ after 24 h of milling. The ρ_D values are comparable to the dislocation densities limit in metal achieved by plastic deformation (10^{16} m^{-2} for edge dislocations). For the milled NC Fe, the maximum ρ_D determined by the Fourier method was about $1.653 \times 10^{16} \text{ m}^{-2}$ [20]. Zhao et al. have reported for NC Fe that ρ_D increases from 0.013×10^{16} to $1.173 \times 10^{16} \text{ m}^{-2}$ with increasing milling time from 0 to 80 h, then decreases slightly to $1.023 \times 10^{16} \text{ m}^{-2}$ (140 h) on further milling [25]. It is obvious that the properties of NC are milling conditions dependent.

Figure 4 shows the q values for different milling times. The theoretical values of q for pure edge and pure screw dislocation are calculated according to the methodology described by Ungár and co-workers [16], for pure iron $q^{\text{edge}} = 1.28$ (pure edge) and $q^{\text{screw}} = 2.67$ (pure screw). These theoretical values are then compared with experimental ones. During the first stage of milling, the screw

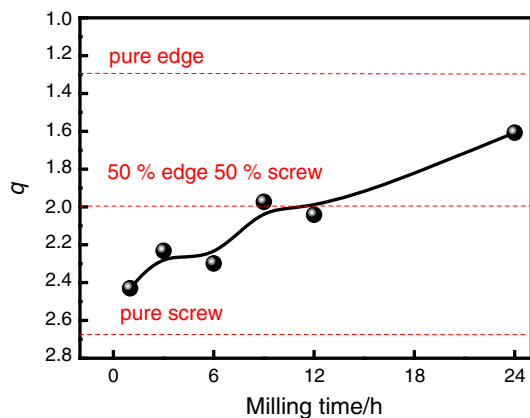


Fig. 4 Nature of dislocations (q) as a function of milling time

Table 3 The calculated screw and edge dislocations fraction

Milling time/h	$\eta_{\text{edge}}/\%$	$\eta_{\text{screw}}/\%$
0	17.266	82.734
3	31.504	68.496
6	26.705	73.295
9	50.029	49.971
12	45.218	54.782
24	76.475	23.525

dislocations are the major component. Their nature changes to about 50–50 for 9 and 12 h of milling but after 24 h of milling, the edge character dominates. The fraction of two dislocation types can be extracted in the following form (Table 3):

$$q = \eta_e q^{\text{edge}} + \eta_s q^{\text{screw}}. \quad (12)$$

The volume fraction associated with GBs, deduced from the Rietveld refinement, increases from 5 to 25 % with decreasing crystallite size from ~ 108 to 12 nm, respectively (Fig. 5). In the NC alloys, the important contribution of the interface which is about 14–20 % of the total Fe has been attributed to the small crystallite size (~ 5 nm) [26]. The GBs thickness can be estimated by considering a spherical shape of grains using the formula:

$$\langle E \rangle = \langle d \rangle \left(\sqrt[3]{\frac{100}{P_G}} - 1 \right), \quad (13)$$

where $\langle d \rangle$ denotes the average crystallite size and P_G is the volume fraction of the crystalline phase (grains). Hence, the estimated GBs thickness of the powders milled for 3, 9, and 24 h is about 0.7, 0.9, and 1.1 nm, respectively. Comparable values (between 0.5 and 1 nm) were obtained by Rawers et al. [27]. In most nanostructured alloys, the estimated thickness of the interfaces was roughly found at

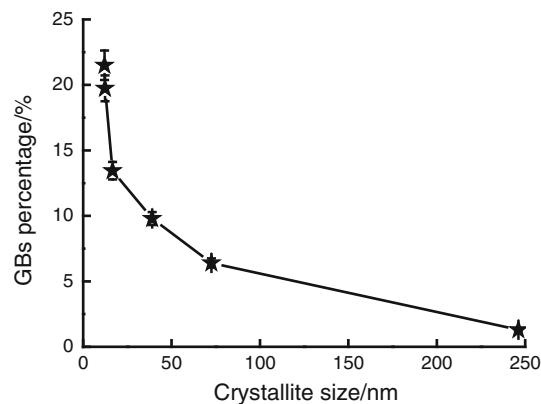


Fig. 5 Evolution of GBs proportion as a function of crystallite size

2–3 atomic layers that is physically consistent with the thickness of the surface layer encountered in non-interacting nanoparticle systems [28]. In the ball milled FeCo powders, the GBs proportions were 18 and 6 % for crystallite size of about 12 and 40 nm, respectively [29].

The slight shift of the diffraction peaks of the bcc-Fe to the smaller (or larger) angles with increasing milling time suggests the variation of the Fe lattice parameter as shown in Fig. 6. The lattice parameter decreases during the first three hours of milling, then it increases to reach a maximum value of about 0.2874 nm after 12 h of milling and decreases again after 24 h of milling. The increase of the lattice parameter during milling can be caused by the increase in the density of dislocations with their characteristic strain fields, whereas the decrease of this parameter (12–24 h) should arise from the grain compression due to the presence of compressive stress fields within the non equilibrium GBs inside the crystallites and, as a result, causes a decrease in the lattice parameter [30]. Another reason may be the oxidation of the finite α -Fe grains which accelerates their fracture [31]. Although during milling neither Fe oxides phases were detected by X-ray studies; however, traces of oxidation and some contaminations (both below the sensitivity limits of the techniques applied) cannot be excluded. The relative deviation of the lattice parameter, a , in comparison to that of the perfect crystal, a_0 , which is defined by $\Delta a = \frac{a-a_0}{a_0}$, reaches as much as 0.31 % after 24 h of milling. This value is comparable to that obtained for the ball milled pure Fe for 50 h in a vibratory Spex 8000 mill with a balls-to-powder mass ratio of 10:1 [32].

The lattice structure of the nanometer-sized crystallites obtained by ball milling deviates evidently from the equilibrium state. The lattice distortion in various NC materials is manifested by a significant change in Debye–Waller parameter (DWP) [33] which is a measure of the displacement of atoms from their ideal positions. It consists of static (DWP_S) and thermal (DWP_T) components.

Fig. 6 Variation of the Fe lattice parameter versus milling time

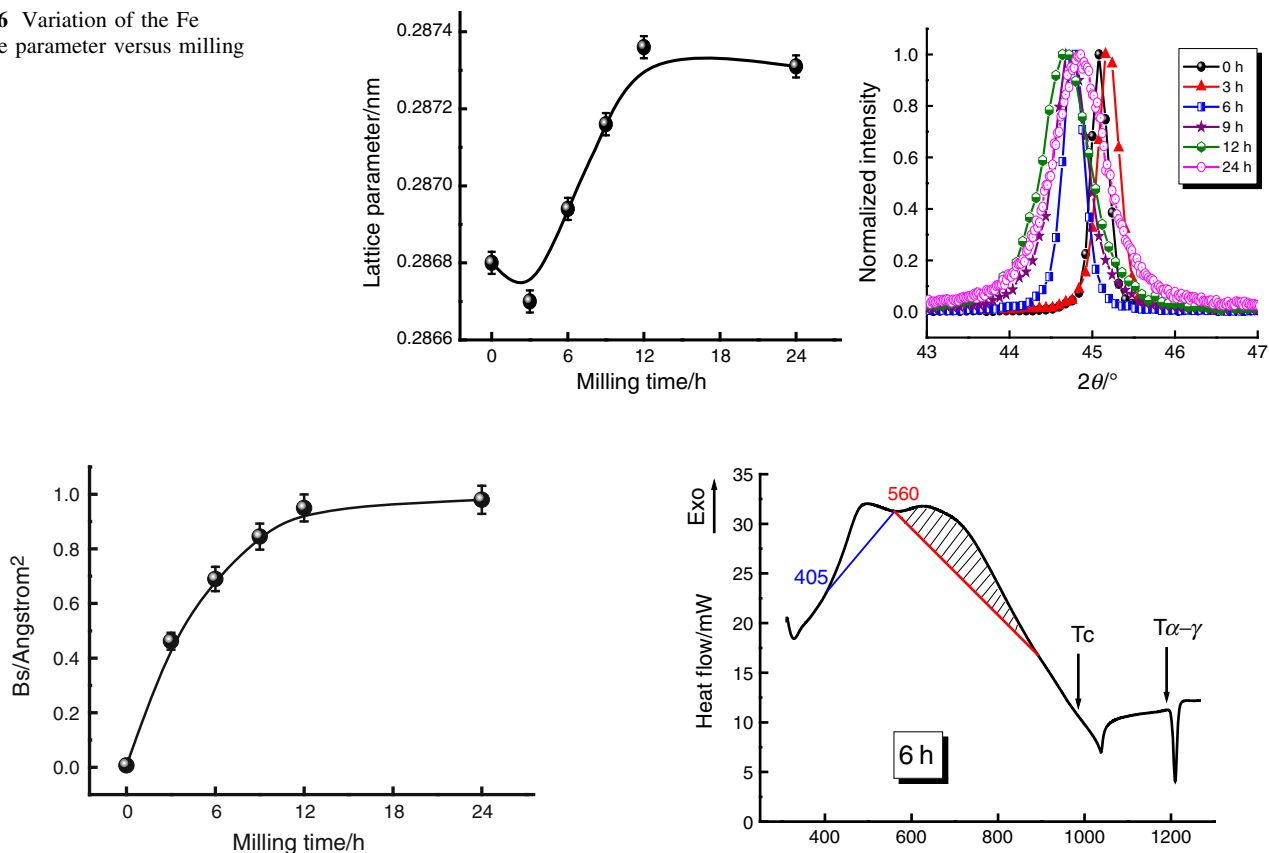


Fig. 7 Static Debye–Waller parameter versus milling time

According to the diffraction theory [34], DWP_S is related to the static displacement of the atom from the equilibrium position caused by defects such as vacancies, interstitials, and dislocations. However, DWP_T is the contribution from the thermal vibrations of the atom around the equilibrium lattice site and is grain-size independent. Since all XRD patterns were taken at ambient temperature, the DWP_T of the Fe is fixed to 0.35 \AA^2 [35]. DWP_S increases with milling time (Fig. 7) to about $0.981 \pm 0.05 \text{ \AA}^2$ after 12 h of milling. It was reported that the static DWP in various NC samples increases by 100–900 % compared to the equilibrium values [33] due to the existence of the lattice distortion in the nanocrystallite lattice.

Thermal stability

Characterization of the thermal properties of materials is a critical step toward understanding the phase formation. When the sample undergoes a transformation (phase transition, recovery or recrystallization), heat is absorbed/evolved which can be accurately measured using DSC [36]. We are mainly interested in the recovery/recrystallization process occurring during heating of the ball milled samples. The DSC scans of the unmilled and milled samples have the same form. Therefore, the DSC scans exhibit a broad

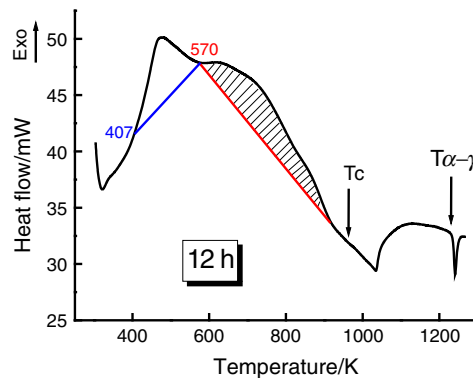
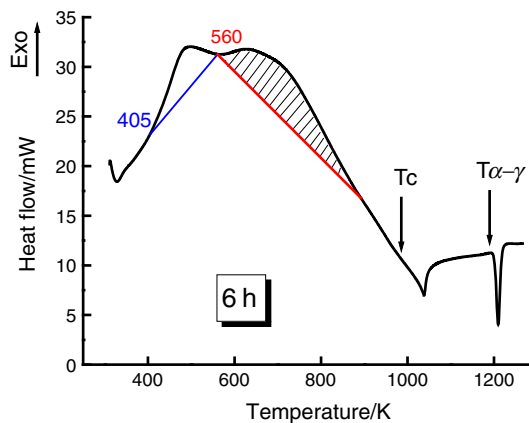


Fig. 8 DSC traces of the milled Fe for 6 and 12 h

exothermic hump composed of two main peaks at about 405 and 560 K and two endothermic peaks (Fig. 8). The first sharp exothermic peak, situated around 450 K, may be attributed to the oxidation of nanostructured Fe powders [37] as confirmed by the mass gain in the TG analysis as shown in Fig. 9. The iron oxide may be due to the contamination of the ball milled powder. The second broad exothermic reaction in the temperature range 560–850 K can be related to recovery, strain relaxation and/or grain growth. Since the transition heats evolving in the atomic reordering and in the grain growth are comparable in value [4], both atomic disorder and nanocrystallite boundaries are thus major sources of

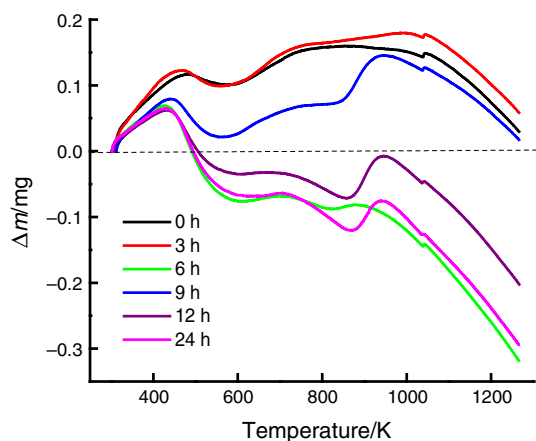


Fig. 9 TG curves of the ball milled Fe powders at different milling times

mechanical energy storage. This behavior is typical for highly deformed materials. The endothermic peaks are related to the ferromagnetic–paramagnetic transition and $\alpha \rightarrow \gamma$ phase transformation, respectively.

The stored enthalpy, ΔH , change during the milling process is estimated from the DSC curve. The area under such a curve between any two temperature limits yields an enthalpy change.

ΔH increases (Fig. 10) with increasing milling time, reaches a maximum value of about 0.839 kJ/mol after 12 h of milling, then decreases slightly to about 0.751 kJ/mol after 24 h of milling. The obtained values which are higher than those reported by Zhao et al. [25] can be attributed to the milling conditions. Similar variations of ΔH were found in the milled NC Ni [24]. It has been reported that the maximum energy departure from equilibrium for particulate materials with a crystallite size of 5 nm was about 10 kJ/mol [38]. The corresponding value for materials with a dislocation density of $\sim 10^{16} \text{ m}^{-2}$ was 1 kJ mol⁻¹. These values show the large amount of stored energy in nanostructured materials. The stored enthalpy corresponds mostly to the defects recovery of the milled powders which includes two contributions: non-equilibrium lattice defects in grains and in the GBs. The former contribution is mainly due to the elastic energy of dislocations situated in the grains, and the latter originates principally from the structural and compositional deviations in GBs region from the inner part of the grains.

By assuming that the milled powders are isotropic (size and strain) and using the obtained dislocation density data, the molar stored energy per molar unit volume, E_{dis} , due to the presence of the dislocations in the powder can be estimated from Eq. (14). The stored energies are typically less than 1 kJ/mol.

$$E_{\text{dis}} = AGb^2 \rho \ln(R_e/r_0), \quad (14)$$

with A is equal to $1/(4\pi(1-\nu))$ and $1/4\pi$ for the edge and screw dislocation, respectively; where ν is the Poisson's

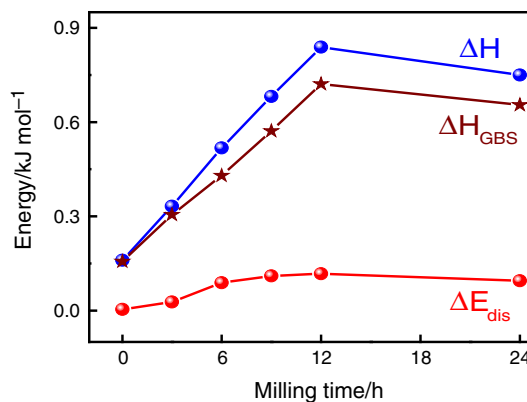


Fig. 10 Stored enthalpy and elastic strain energy variation versus milling time

ratio equals to 0.291 for Fe [28]; G is the shear modulus equal to $8.073 \times 10^{10} \text{ N m}^{-2}$ [39]. R_e and r_0 are the outer and the inner cut-off radii of the dislocations, respectively. The inner cut-off radius can be assumed equal to the length of Burger vector ($r_0 = b$). R_e in NSM would far exceed crystallite size. Therefore, since the crystallite size is (hkl) dependent, the average crystallite size (d) is considered as the outer cut-off radius of the dislocations. The interaction energy of the dislocations can be neglected since, for NC materials, individual grains contain only a few amounts of dislocations [20]. Since the grains contain screw and edge dislocations in different proportions, the constant A must be averaged for the two types of dislocations as

$$A = \frac{1}{4\pi} \left(\frac{\eta_e}{1-\nu} + \eta_s \right). \quad (15)$$

Figure 10 shows the variation of different energies versus milling time. It can be seen that ΔE_{dis} attains a maximum value of about 0.117 kJ/mole after 12 h of milling (Fig. 10) but it yields only a very small fraction of ΔH , suggesting that most of ΔH arise from the GBs. Hence, The GBs enthalpy release, ΔH_{GBs} can be estimated by separating ΔE_{dis} from ΔH . In fact, it can be seen that the ΔH_{GBs} yield a dominant part ($\sim 78\text{--}90\%$) in ΔH which is in good agreement with the increase of GBs fraction during milling process. The atoms at GBs may have a slight different coordination number compared to those in the grain, and the bonds are also distorted [40]. Above 12 h of milling, the grain size remains constant while the GBs enthalpy decreases. This behavior can be explained by the fact that further milling results in a GBs relaxation which causes variations in the thermal and structural properties.

The variation of Curie temperature, T_c , and the $\alpha \rightarrow \gamma$ transition temperature, $T_{\alpha \rightarrow \gamma}$, during the milling process are shown in Fig. 11. T_c decreases with increasing milling time by about 41 K compared to that of bulk iron after 24 h. However, the $\alpha \rightarrow \gamma$ transformation temperature increases to 1,230 K after 24 h of milling. The decrease of Curie

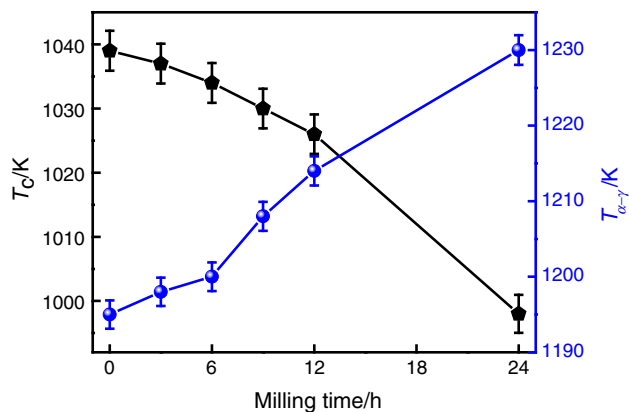


Fig. 11 Variation of T_c and $T_{\alpha \rightarrow \gamma}$ against milling time

temperature might be due to the grain size refinement. In fact, if the grain sizes are small enough, the structural distortions associated with the surfaces or interfaces can lower the Curie temperature [41]. The structural distortions can be confirmed by the Fe lattice parameter increasing with the milling time. It has been reported on far from-equilibrium nanostructured metals that interfaces present a reduced atomic coordination and a wide distribution of interatomic spacing compared to the crystals and consequently, the atomic arrangement at the GBs may be considered close to the amorphous configuration and should therefore alter the Curie temperature [42]. For most observations in the literature, the Curie temperature does not deviate strongly from that of the bulk materials [43]. According to the variations of both the Curie temperature and the $\alpha \rightarrow \gamma$ -Fe phase transformation temperature ($T_{\alpha \rightarrow \gamma}$), it is obvious that the paramagnetic bcc γ -Fe domain is extended by about 75 K at the expense of both magnetic bcc α -Fe and nonmagnetic fcc γ -Fe as compared to coarse grained bcc α -Fe.

Conclusions

Nanostructured Fe powders were obtained by ball milling in a high-energy planetary ball mill (Fritsch Pulverisette P7). The increase of the GBs surface area can be linked to the crystallite size reduction and the increase of the dislocation density. The screw dislocations are the major component in the early stage of milling. Their nature changes to 50–50 during the intermediate stage of milling and after 24 h of milling, the screw character dominates again.

The bcc α -Fe paramagnetic temperature domain is extended by about 75 K at the expense of both magnetic bcc α -Fe and nonmagnetic fcc γ -Fe as the milling process progresses. The Curie temperature decreases by about 41 K as compared to bulk iron.

References

- Zhu X, Birringer R, Herr U, Gleiter H. X-ray diffraction studies of nanometer-sized crystalline materials. *Phys Rev B*. 1987;35:9085–90.
- Alleg S, Souilah S, Suñol JJ. Thermal stability of the nanostructured powder mixtures prepared by mechanical alloying. In: Elkordy AA, editor. Applications of calorimetry in a wide context—differential scanning calorimetry, isothermal titration calorimetry and microcalorimetry. Vienna: InTech Publisher; 2013. p. 21–48.
- Alleg S, Kartout S, Ibrir M, Azzaza S, Fenineche NE, Suol JJ. Magnetic, structural and thermal properties of the Finemet-type powders prepared by mechanical alloying. *J Phys Chem Sol*. 2013;74:550–7.
- Azzaza S, Alleg S, Suñol JJ. Phase transformation in the ball milled $\text{Fe}_{31}\text{Co}_{31}\text{Nb}_8\text{B}_{30}$ Powders. *Adv Mater Phys Chem*. 2013;3:90–100.
- Del Bianco L, Hernando A, Fiorani D. Spin-glass-like behavior in nanocrystalline Fe. *Phys Stat Sol (a)*. 2002;189:533–6.
- Alleg S, Azzaza S, Bensalem R, Sunol JJ, Khene S, Fillion G. Magnetic and structural studies of mechanically alloyed $(\text{Fe}_{50}\text{Co}_{50})_{62}\text{Nb}_8\text{B}_{30}$ powder mixtures. *J Alloys Compd*. 2009;482:86–9.
- Haubold T, Krauss W, Gleiter H. EXAFS studies on nanocrystalline tungsten. *Phil Mag Lett*. 1991;63:245–7.
- Lutterotti L. MAUD CPD. Newsletter (IUCr) 2000; 24.
- Rietveld HM. A profile refinement method for nuclear and magnetic structures. *J Appl Cryst*. 1969;2:65.
- Young RA. The Rietveld method. 1st ed. Oxford: Oxford University Press; 1996.
- Young RA, Wiles DB. Profile shape functions in Rietveld refinements. *J Appl Cryst*. 1982;15:430–8.
- Caglioti G, Paoletti A, Ricci FP. Choice of collimators for a crystal spectrometer for neutron diffraction. *Nucl Instrum Methods*. 1958;35:223–8.
- Popa NC. The (hkl) dependence of diffraction-line broadening caused by strain and size for all laue groups in Rietveld refinement. *J Appl Cryst*. 1998;31:176–80.
- Popa NC. Texture in Rietveld refinement. *J Appl Cryst*. 1992;25:611.
- Williamson GK, Smallman RE. Dislocation densities in some annealed and cold-worked metals from measurements on the X-ray Debye–Scherrer spectrum. *Phil Mag*. 1956;1:34–45.
- Ungár T, Dragomir I, Rêvész Á, Borbely A. The contrast factors of dislocations in cubic crystals: the dislocation model of strain anisotropy in practice. *J Appl Cryst*. 1999;32:992–1002.
- Borbely A, Dragomir I, Ribárik G, Ungár T. Computer program ANIZC for the calculation of diffraction contrast factors of dislocations in elastically anisotropic cubic, hexagonal and trigonal crystals. *J Appl Cryst*. 2003;36:160–2.
- Scardi P, Leoni M. Fourier modelling of the anisotropic line broadening of X-ray diffraction profiles due to line and plane lattice defects. *J Appl Cryst*. 1999;32:671–82.
- Dong YH, Scardi P. MarqX: a new program for whole-powder-pattern fitting. *J Appl Cryst*. 2000;33:184–9.
- Rêvész Á, Ungár T, Borbely A, Lendvai J. Dislocations and grain size in ball milled iron powder. *Nanostruct Mater*. 1996;7:779–88.
- Mallow TR, Koch CC. Grain growth in nanocrystalline iron prepared by mechanical attrition. *Acta Mater*. 1997;45:2177–86.
- Guérault H, Greneche JM. Microstructural modeling of nanostructured fluoride powders prepared by mechanical milling. *J Phys*. 2000;12:4791–8.

23. Laala-Bouali H, Bentayeb F-Z, Louidi S, Guo X, Tria S, Suñol JJ. X-ray line profile analysis of the ball milled Fe–30Co alloy. *Adv Powd Technol.* 2013;24:168–74.
24. Eckert J, Holzer JC, Kill CE III, Johnson WL. Synthesis and characterization of ball-milled nanocrystalline fcc metals. *J Mater Res.* 1992;7:1751–61.
25. Zhao ZH, Sheng HW, Lu K. Microstructure evolution and thermal properties in nanocrystalline Fe during mechanical attrition. *Acta Mater.* 2001;49:365–75.
26. Slawska-Waniewska A, Grafoute M, Greneche JM. Magnetic coupling and spin structure in nanocrystalline iron powders. *J Phys.* 2006;18:2235–48.
27. Rawers J, Cook D. Influence of attrition milling on nano-grain boundaries. *Nanostruct Mater.* 1999;11(3):331–42.
28. Greneche JM, Ślawska-Waniewska A. About the interfacial zone in nanocrystalline alloys. *J Magn Magn Mater.* 2000;215–216:264–7.
29. Delshad Chermahini M, Shokrollahi H. Milling and subsequent thermal annealing effects on the microstructural and magnetic properties of nanostructured Fe₉₀Co₁₀ and Fe₆₅Co₃₅ Powders. *J Alloys Compd.* 2009;480:161–6.
30. Zhang K, Alexandrov IV, Lu K. The X-ray diffraction study on a nanocrystalline Cu Processed by Equal-Channel Angular Pressing. *Nanostruct Mater.* 1997;9:347–50.
31. Mhadhbi M, Khitouni M, Azabou M, Kolsi AW. Characterization of Al and Fe nanosized powders synthesized by high energy mechanical milling. *Mater Charact.* 2008;59:944–50.
32. Ram S, Fecht HJ. Millimeter sized ferromagnetic Fe-clusters: Formation by mechanical attrition, microstructure and magnetic properties. *Mat Trans JIM.* 2000;41:754–60.
33. Lu K, Zhao YH. Experimental evidences of lattice distortion in nanocrystalline materials. *Nanostruct Mater.* 1999;12:559–62.
34. Krivoglaz M. *Theory of X-ray and thermal-neutron scattering by real crystals*. New York: Plenum Press; 1969.
35. Dubrovinsky LS, Dubrovinskaia NA, Saxena SK, Rekh S, Le Bihan T. Aggregate shear moduli of iron up to 90 GPa and 1,100 K. *J Alloys Compd.* 2000;297:156–61.
36. Antoszewska M, Wasiak M, Gwizdała T, Sovak P, Moneta M. Thermal induced structural and magnetic transformations in Fe_{73.5-x}Ce_{x = 0, 3, 5, 7}Si_{13.5}B₉Nb₃Cu₁ amorphous alloy. *J Therm Anal Calorim.* 2014;115:1381–6.
37. Lysenko EN, Surzhikov AP, Zhuravkov SP, Vlasov VA, Pustovalov AV, Yavorovsky NA. The oxidation kinetics study of ultrafine iron powders by thermogravimetric analysis. *J Therm Anal Calorim.* 2014;115:1447–52.
38. Fecht HJ. Nanostructured materials: processing, properties and potential applications. In: Koch CC, editor. Noyes publications. Norwich: New York; 2002. p. 73–113.
39. Speich GR, Schwoeble AJ, Leslie WC. Elastic constants of binary iron-base alloys. *Met Trans.* 1972;3:2031–7.
40. Stern EA, Siegel RW, Newville M, Sanders PG, Haskell D. Are nanophase grain boundaries anomalous? *Phys Rev Lett.* 1995;75:3874–7.
41. Suñol JJ, González A, Escoda L, Vilaró A. Curie temperature in Fe(Ni)Nb based mechanically alloyed materials. *J Therm Anal Calorim.* 2005;80:257–61.
42. Lu K. The thermal instability of nanocrystalline Ni–P materials with different grain sizes. *Nanostruct Mater.* 1993;2:643–52.
43. Krill CE, Merzoug F, Krauss W, Birringer R. Magnetic properties of nanocrystalline Gd and W/Gd. *Nanostruct Mater.* 1997;9:455–60.